

AD-A163 210

PARTICLE AND WAVE DYNAMICS DURING PLASMA INJECTIONS(U)

1/1

AEROSPACE CORP EL SEGUNDO CA SPACE SCIENCES LAB

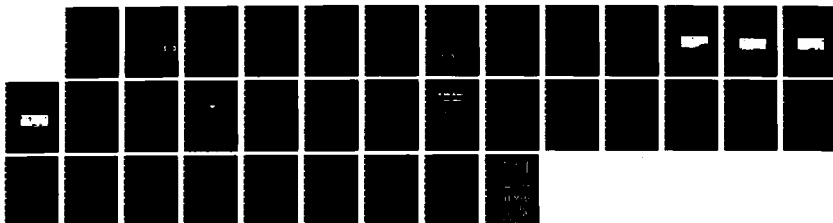
H C KOONS ET AL 15 JUL 85 TR-0084A(5940-06)-3

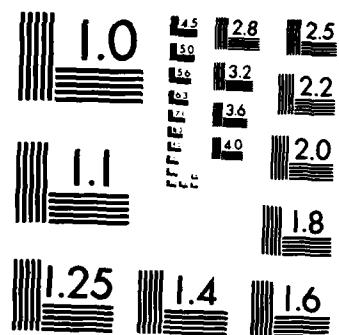
UNCLASSIFIED

SD-TR-85-51 F04701-83-C-0084

F/G 4/1

NL





MICROCOPY RESOLUTION TEST CHART
NATIONAL BUREAU OF STANDARDS-1963-A

AD-A163 210

Particle and Wave Dynamics During Plasma Injections

Prepared by

H. C. KOONS and J. F. FENNELL
Space Sciences Laboratory
Laboratory Operations
The Aerospace Corporation
El Segundo, CA 90245

15 July 1985

APPROVED FOR PUBLIC RELEASE;
DISTRIBUTION UNLIMITED

Prepared for

SPACE DIVISION
AIR FORCE SYSTEMS COMMAND
Los Angeles Air Force Station
P.O. Box 92960, Worldway Postal Center
Los Angeles, CA 90009-2960

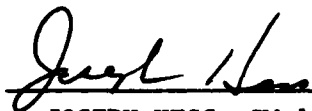
This report was submitted by The Aerospace Corporation, El Segundo, CA 90245, under Contract No. F04701-83-C-0084 with the Space Division, P.O. Box 92960, Worldway Postal Center, Los Angeles, CA 90009-2960. It was reviewed and approved for The Aerospace Corporation by H. R. Rugge, Director, Space Sciences Laboratory. Lieutenant Douglas R. Case, SD/YCM, was the project officer for the Mission- Oriented Investigation and Experimentation (MOIE) Program.

This report has been reviewed by the Public Affairs Office (PAS) and is releasable to the National Technical Information Service (NTIS). At NTIS, it will be available to the general public, including foreign nationals.

This technical report has been reviewed and is approved for publication. Publication of this report does not constitute Air Force approval of the report's findings or conclusions. It is published only for the exchange and stimulation of ideas.



DOUGLAS R. CASE, Lt, USAF
MOIE Project Officer
SD/YCM



JOSEPH HESS, GM-15
Director, AFSTC West Coast Office
AFSTC/WCO OL-AB

UNCLASSIFIED

SECURITY CLASSIFICATION OF THIS PAGE (When Data Entered)

REPORT DOCUMENTATION PAGE		READ INSTRUCTIONS BEFORE COMPLETING FORM
1. REPORT NUMBER SD-TR-85-51	2. GOVT ACCESSION NO.	3. RECIPIENT'S CATALOG NUMBER
4. TITLE (and Subtitle) PARTICLE AND WAVE DYNAMICS DURING PLASMA INJECTIONS		5. TYPE OF REPORT & PERIOD COVERED
		6. PERFORMING ORG. REPORT NUMBER TR-0084A(5940-06)-3
7. AUTHOR(s) H. C. Koons and J. F. Fennell		8. CONTRACT OR GRANT NUMBER(s) F04701-83-C-0084
9. PERFORMING ORGANIZATION NAME AND ADDRESS The Aerospace Corporation El Segundo, Calif. 90245		10. PROGRAM ELEMENT, PROJECT, TASK AREA & WORK UNIT NUMBERS
11. CONTROLLING OFFICE NAME AND ADDRESS Space Division Los Angeles Air Force Station Los Angeles, Calif. 90009		12. REPORT DATE 15 July 1985
		13. NUMBER OF PAGES 29
14. MONITORING AGENCY NAME & ADDRESS (if different from Controlling Office)		15. SECURITY CLASS. (of this report) Unclassified
		15a. DECLASSIFICATION/DOWNGRADING SCHEDULE
16. DISTRIBUTION STATEMENT (of this Report) Approved for public release; distribution unlimited.		
17. DISTRIBUTION STATEMENT (of the abstract entered in Block 20, if different from Report)		
18. SUPPLEMENTARY NOTES		
19. KEY WORDS (Continue on reverse side if necessary and identify by block number) Magnetosphere Plasma sheet Substorms Wave-particle interactions		
20. ABSTRACT (Continue on reverse side if necessary and identify by block number) The SCATHA satellite measures particle and wave parameters as it moves out-bound on the dusk side from the plasmasphere into the plasma sheet. In many cases plasma waves are not observed in the quiescent plasma sheet prior to a plasma injection. The electron distribution function prior to entry into the plasma sheet is a nearly isotropic soft spectrum $J(E) \sim 1/E$. Just inside the plasma sheet the spectrum begins to harden and becomes anisotropic, $J_{\perp} > J_{\parallel}$. As the satellite penetrates deeper into the plasma		

DD FORM 1473 (FACSIMILE) AIR FORCE 86145/6-1-86 - 100

UNCLASSIFIED
SECURITY CLASSIFICATION OF THIS PAGE (When Data Entered)

UNCLASSIFIED

SECURITY CLASSIFICATION OF THIS PAGE(When Data Entered)

19. KEY WORDS (Continued)

27-500 2 27-500 92-100

20. ABSTRACT (Continued)

→ sheet the spectrum further hardens, especially near $\alpha \sim 90^\circ$. At the injection the electron spectrum drastically hardens and often becomes peaked in the keV energy range. The pitch angle anisotropy is further enhanced in favor of J_z . The plasma wave emissions onset occurred at the time of the injection. Whistler-mode waves are observed below the electron cyclotron frequency. Electrostatic waves are detected in bands between the electron cyclotron frequency harmonics. *Report 282 - 2 to 10/26/19*

page 10

UNCLASSIFIED

SECURITY CLASSIFICATION OF THIS PAGE(When Data Entered)

PREFACE

The authors are indebted to E. Whipple of UCSD for the particle spectrograms and B. Ledley of GSFC for the magnetometer data.

We would like to thank all of the people who made this study possible. Special thanks go to L. Friesen, R. Maulfair and D. Croley for providing support of the data reduction and analysis.

CONTENTS

PREFACE.....	1
I. INTRODUCTION.....	7
II. NARROWBAND VLF DATA.....	19
III. ELECTRON DISTRIBUTING FUNCTIONS.....	23
IV. SUMMARY.....	31
REFERENCES.....	33

DTIC
ELECTE
S **D**
JAN 22 1986
B

Accession For	
NTIS GRA&I	<input checked="" type="checkbox"/>
DTIC TAB	<input type="checkbox"/>
Unannounced	<input type="checkbox"/>
Justification	
By	
Distribution/	
Availability Codes	
Dist	Avail and/or Special
A-1	

FIGURES

1.	SCATHA Wave and Particle Data Showing the Entry into the Plasma Sheet and the Plasma Injection on April 18, 1979.....	9
2.	Same as Fig. 1 for May 1, 1979.....	10
3.	Same as Fig. 1 for May 20, 1979.....	11
4.	Same as Fig. 1 for May 22, 1979.....	12
5.	Location of the SCATHA Satellite in a Radius vs. Local Time Coordinate Frame at the Times of Plasma-sheet Entries and Plasma Injections described in this Paper.....	15
6.	The Magnetic Field Intensity Time Profiles for the Four Cases Studied.....	16
7.	Gray Scale Spectrograms of the VLF Wave Spectrum During the Plasma Injections Described in this Paper.....	20
8.	Iso-distribution Function Contours in Velocity Space Taken on April 18, 1979.....	24
9.	Same as Fig. 8 for May 1, 1979.....	25
10.	Same as Fig. 8 for May 20, 1979.....	26
11.	Same as Fig. 8 for May 22, 1979.....	27
12.	Electron Energy Spectra.....	28
13.	Electron Pitch-angle Distributions Taken near 0325 UT on May 1, 1979.....	30

I. INTRODUCTION

Plasma sheet electrons are precipitated into the atmosphere on auroral field lines creating the diffuse aurora. The strong pitch angle diffusion is believed to be caused by electrostatic electron cyclotron waves [Kennel et al., 1970 and Lyons, 1974]. The theory has been reviewed by Kennel and Ashour-Abdalla [1982].

There have been few simultaneous observations of wave spectra and electron distribution functions within the plasma sheet. Kurth et al. [1980] report a positive-sloped feature in the electron velocity distributions at a pitch angle $\alpha = 90^\circ$ during an intense electrostatic wave event detected by ISEE 1. The feature did not appear in distributions taken before or after the waves were observed. Rönmark et al. [1978] studied an event observed by GEOS-1 when $(n + 1/2) f_c^-$ and upper hybrid emissions were observed in the presence of a hot loss-cone component of the electron distribution.

Kurth et al. [1979] report intense electrostatic waves near the plasma-pause and close to the upper-hybrid resonance frequency. Three sources of free energy were found: (1) a small temperature anisotropy, (2) a loss-cone distribution in the hot electron population and (3) in one case a small hump in the tail of the distribution function in v_\perp . They distinguish these intense $(n + 1/2) f_c^-$ emissions near f_{UHR} from the $(n + 1/2) f_c^-$ type waves considered in this paper.

Electron distribution functions observed by the SCATHA satellite when intense electrostatic waves are present between the lower harmonics of the electron cyclotron frequency rarely have the positive-sloped feature reported by Kurth et al. [1980] and usually have a much smaller loss-cone feature than the one reported by Rönmark et al. [1978].

Electrostatic waves are often absent in the plasma sheet in the dusk to midnight region before a substorm. This is an important point that apparently has not been reported.

Our objective in this report is to clarify the temporal changes of the particles and waves in the plasma sheet. For this purpose we examine electron dynamics and plasma wave phenomena in the plasma sheet before, during, and after four typical injections. We define an injection to be the abrupt transport inward of plasma sheet electrons during the energy release phase of a magnetospheric substorm. We have chosen four examples in which the SCATHA satellite crosses a quasi-static, plasma-sheet boundary well before the plasma injection occurs. The location of this plasma-sheet boundary depends primarily upon the intensity of the electric field across the magnetosphere in an equilibrium convection model [Kivelson et al., 1980]. These examples allow us to study the particle and wave distribution functions under the following circumstances: first, in the outer magnetosphere just after entry into the plasma sheet; second, in the plasma sheet well after entry but before an injection; third, in the plasma sheet just before an injection and finally in the plasma sheet following an injection.

For this study we have the following simultaneous particle, wave, and magnetic field data available: 1) particle distribution functions from the Aerospace electrostatic analyzers covering the energy range from 20 eV to 20 keV ; 2) particle spectrograms from the UCSD electrostatic analyzers covering the energy range from ~ 1 eV to 81 keV [Olsen, 1981; Mauk and McIlwain, 1975]; 3) spectrograms of the Aerospace broadband VLF data covering the frequency range from 100 Hz to 5 kHz [Koons, 1981]; 4) narrowband VLF data covering the frequency range from 400 Hz to 300 kHz; and 5) magnetic field data from the GSFC three-axis magnetometer. The instruments are described by Fennell [1982].

Electron spectrograms of the four cases chosen for the study are shown at the bottom of Figs. 1-4. Universal times for each case are listed in Table 1.

On April 18, 1979 (Fig. 1 - Case A) the quasi-static, plasma-sheet boundary was first encountered at the lowest energy at about 0740 UT. The satellite penetrated into the plasma sheet crossing the Alfvén boundaries of successively higher energy electrons until a plasma injection occurred near 0905 UT.

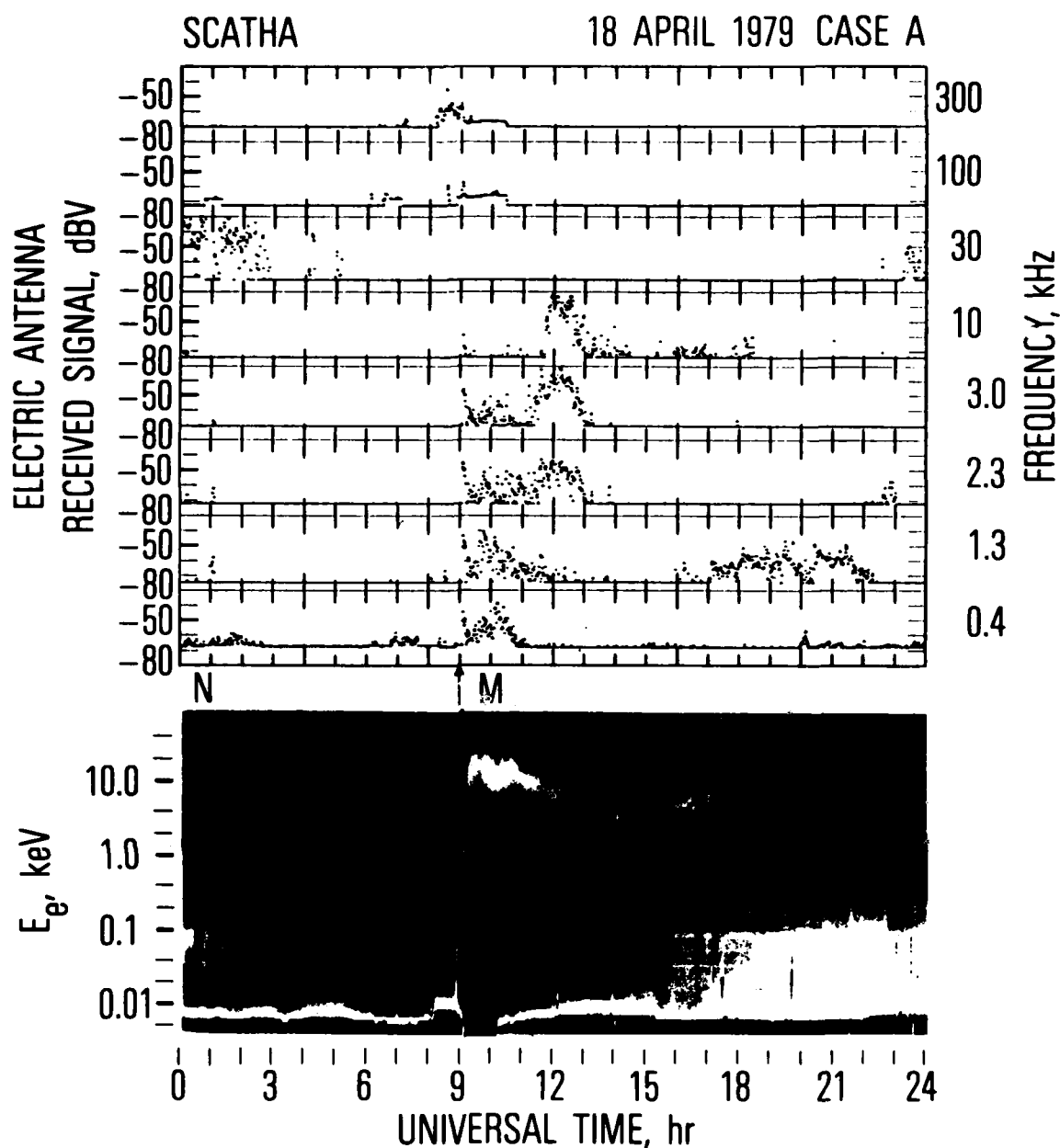


Fig. 1. SCATHA wave and particle data showing the entry into the plasma sheet and the plasma injection on April 18, 1979. The top eight panels are electric field amplitudes in 15 percent bandwidth frequency channels centered at 0.4, 1.3, 2.3, 3.0, 10, 30, 100, and 300 kHz. The lower panel is a gray scale spectrogram showing electron energy fluxes from one of the UCSD particle detectors on SCATHA as a function of energy (vertical axis) and Universal Time (horizontal axis). An increase in lightness corresponds to an increase in electron energy flux. Between the panels the letter N locates local noon and M local midnight at the satellite.

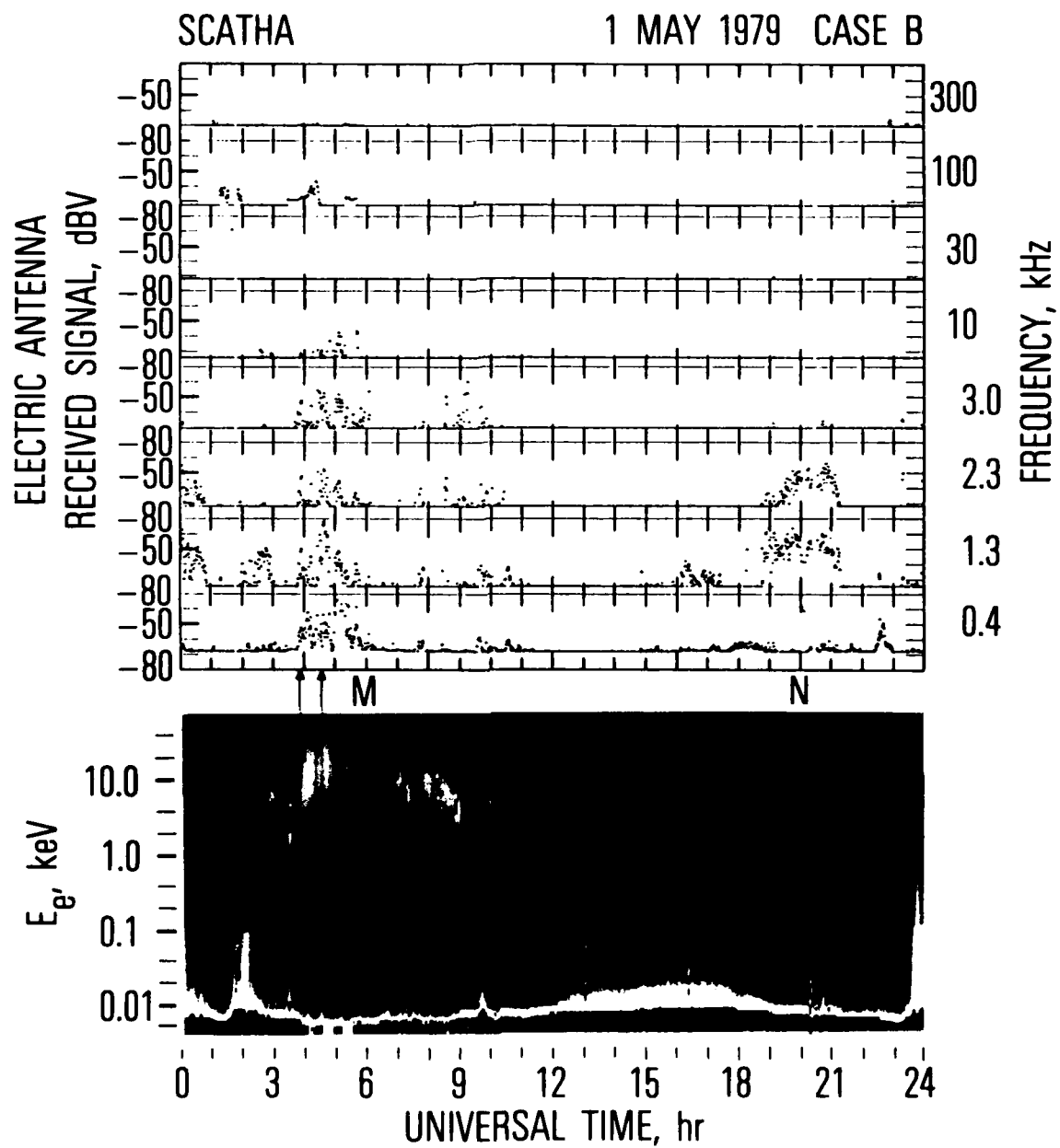


Fig. 2. Same as Fig. 1 for May 1, 1979.

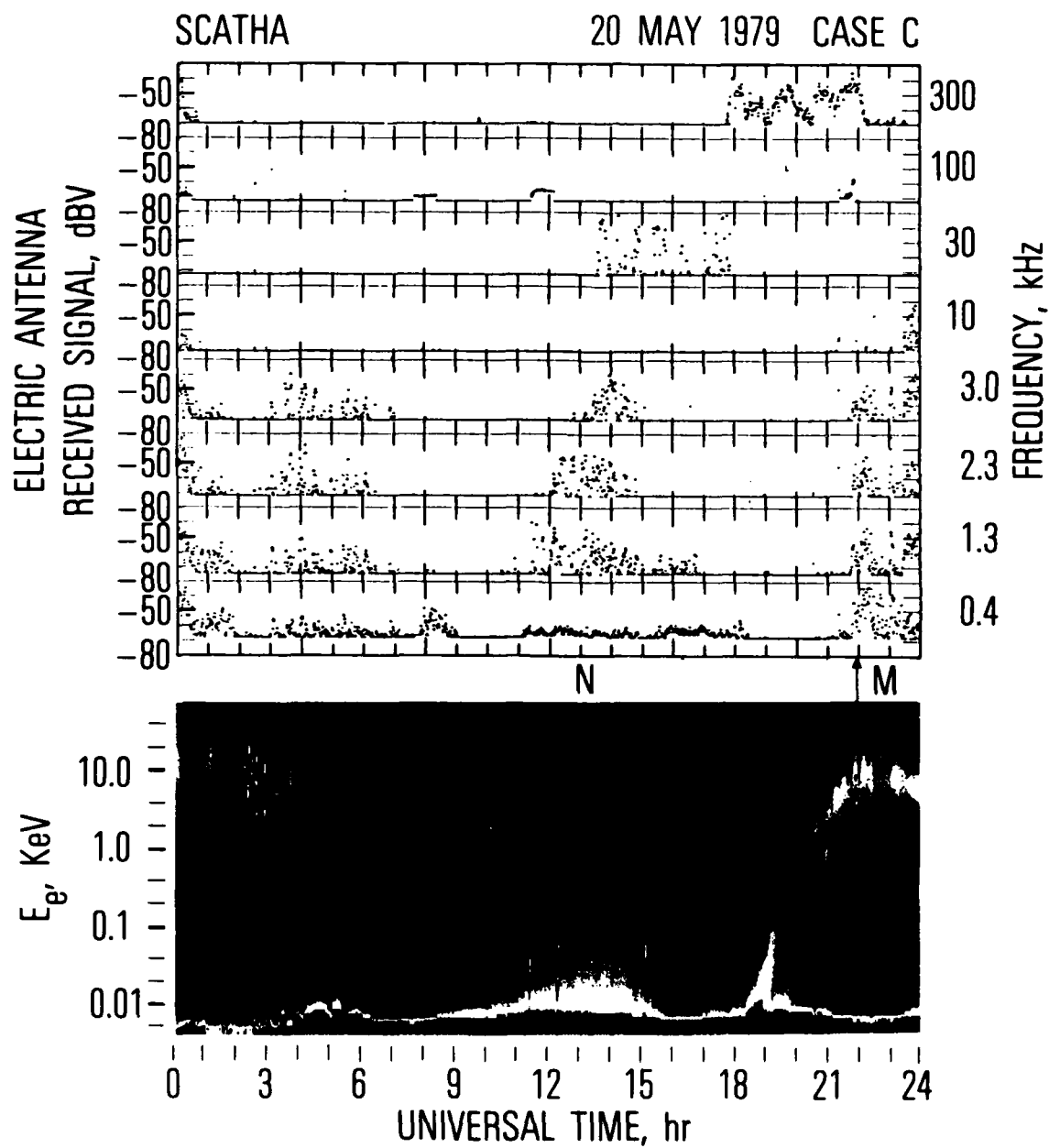


Fig. 3. Same as Fig. 1 for May 20, 1979.

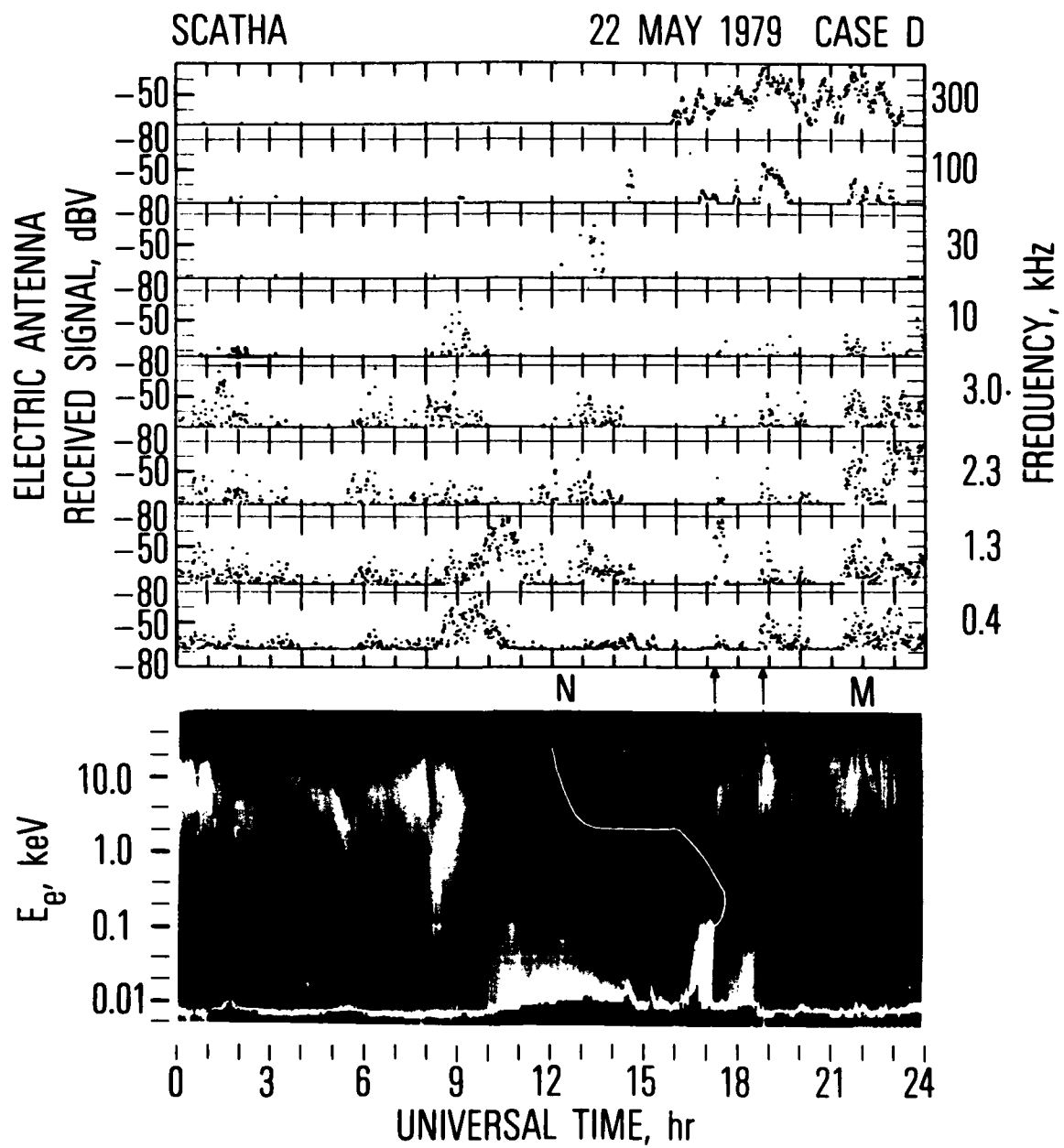


Fig. 4. Same as Fig. 1 for May 22, 1979.

Table 1. Universal times for the examples
presented in this paper.

<u>Case</u>	<u>Date, 1979</u>	Plasma Sheet	Plasma	Invariant	Local
		<u>Entry, UT</u>	<u>Injections, UT</u>	<u>Latitude, deg</u>	<u>Time, hr</u>
A	18 April	07:40	09:05	67.7	23.4
B	1 May	01:40	03:50	67.9	22.6
B	1 May		04:25	68.2	23.2
C	20 May	18:30	21:45	68.9	23.3
D	20 May	16:15	17:00	66.2	18.7
D	22 May		18:45	67.7	20.9

On May 1, 1979 (Fig. 2 - Case B) the low-energy plasma-sheet boundary was encountered at approximately 0140 UT. The satellite penetrated into the plasma sheet detecting two plasma injections at 0350 and 0425 UT.

On May 20, 1979 (Fig. 3 - Case C) the low-energy, plasma-sheet boundary was crossed at 1830 UT. The plasma injection was detected at 2145 UT. This injection is not as prominent on the spectrogram as the others because the satellite had already crossed the Alfvén boundaries of electrons with energies up to 10 keV.

In the final case (Fig. 4 - Case D), on May 22, 1979, the satellite crossed into the plasma sheet at about 1615 UT. Two injections were detected, the first near 1700 UT and the second at 1845 UT.

The orbit segments for these four cases are shown in Fig. 5. The spatial position of the satellite at each injection is indicated by the dots. The invariant latitude and local time is given in Table 1. A comparison of these locations with the auroral oval which is also shown schematically in Fig. 5 shows that all of these injections probably occurred on field lines associated with the diffuse aurora.

The geomagnetic field data for the four cases are shown in Fig. 6. The magnitude of the total field is plotted together with a model field. The model field combines an Olson-Pfitzer [1974] model for current sources external to the earth with a Barraclough [Barraclough et al., 1975] model for the field of internal origin. The magnetic field was moderately disturbed during each of the four time periods. In all four cases there was an abrupt change in the magnitude and geometry of the geomagnetic field at the satellite at the time of each plasma injection. The geomagnetic field was more tail like prior to the injection and became more dipolar during and after the injection. There were also increases in AE at the injection times [World Data Center, 1982]. Examination of the satellite motion shows that satellite latitudinal motion was $\lesssim 1^\circ$ during a one hour interval about the injection. The radial motion was also small (0.2 to 0.3 R_E). We conclude from these magnetic field signatures and the constancy of the satellite latitude that the four cases

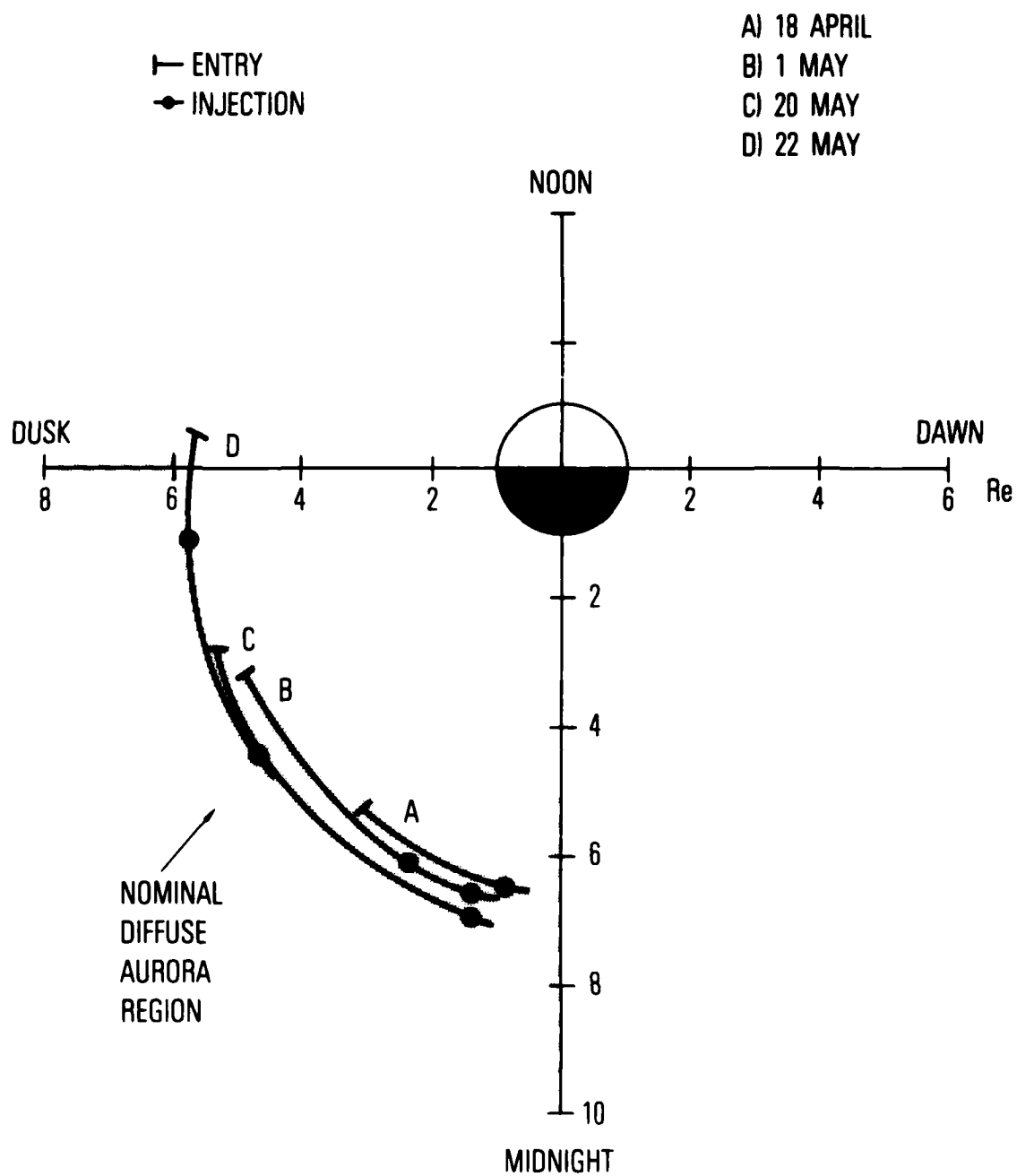


Fig. 5. Location of the SCATHA satellite in a radius vs. local time coordinate frame at the times of plasma-sheet entries and plasma injections described in this paper. The stippled area shows the position of the diffuse auroral region [from Akasofu and Kan, 1980].

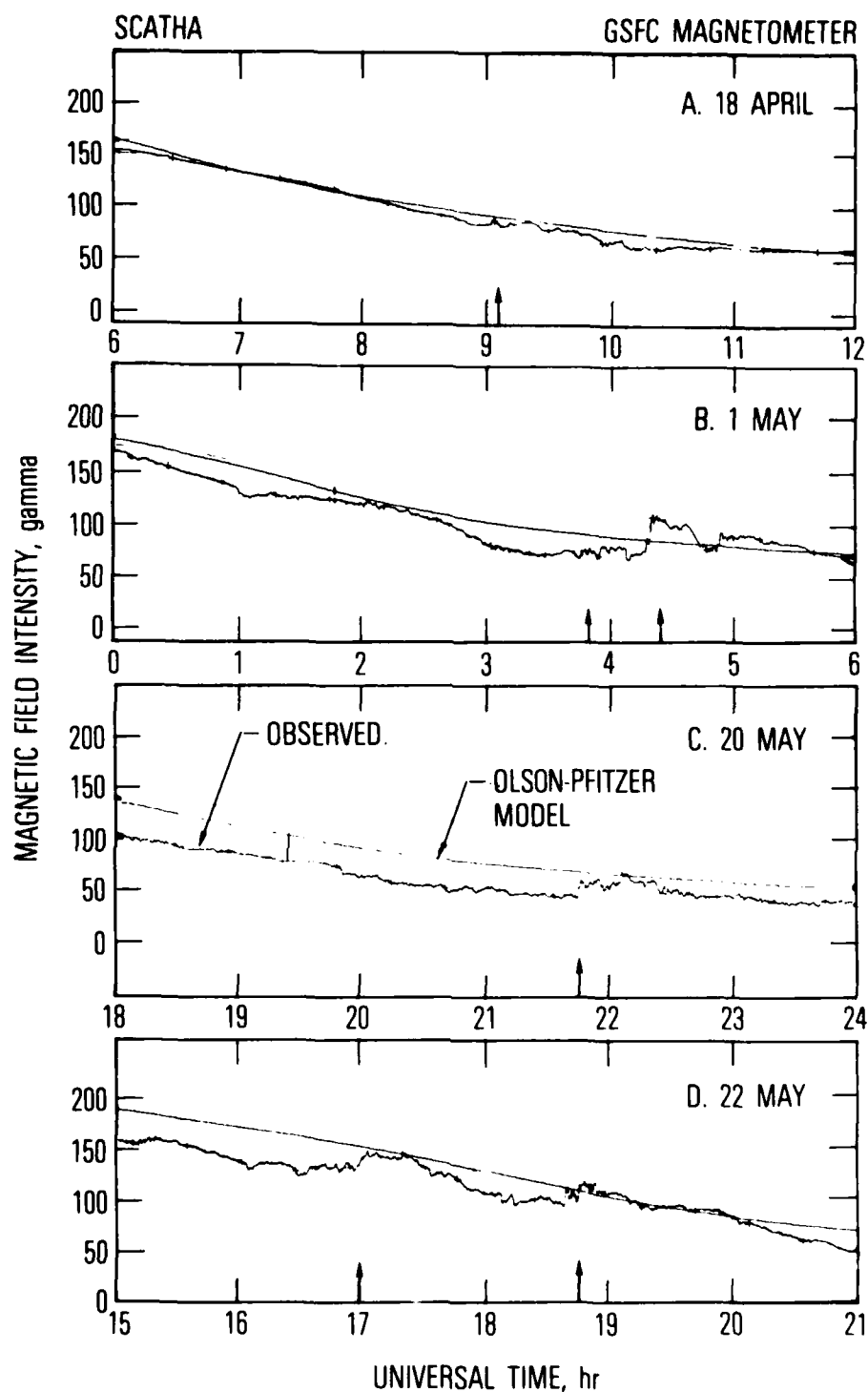


Fig. 6. The magnetic field intensity time profiles for the four cases studied. The smooth solid line is the predicted value using the Olson-Pfitzer field model with tilt [Olson and Pfitzer, 1974]. The thin line represents the observed field values from the GSFC magnetometer.

correspond to plasma injections accompanied by rapid changes in the geomagnetic field configuration [Kivelson, 1980], rather than the satellite crossing an established boundary within the plasma sheet.

In Case A the magnitude of the magnetic field change is much smaller than in the other three examples. Examination of the individual components showed that the largest short term (<2 min) variation occurred in the horizontal component of the magnetic field. This confirms that a reconfiguration of the field occurred during the substorm. Following the initial injection, the satellite crossed the magnetic equator as seen in the radial component, which changed from radially outward (positive sign) to radially inward (negative sign).

The first encounter with the plasma in Case B at 0350 UT is similar to the encounter in Case A. The second encounter in Case B at 0420 UT and the encounters in Cases C and D were each accompanied by obvious step changes in the magnitude of the magnetic field. Below we show that each of the cases displayed similar particle and wave behavior.

II. NARROWBAND VLF DATA

Data from the narrowband VLF receiver for each of the four cases are also shown in Figures 1-4. Only data from the electric antenna are shown.

The first important point to note is the general absence of emissions below 10 kHz between the time the low-energy plasma-sheet boundary is first crossed until the plasma injection occurs. The only exceptions are the presence of weak electrostatic electron cyclotron harmonic emissions evident in the broadband data from Cases A and B and an electromagnetic signal between 0200-0300 UT at 1.3 kHz in Fig. 2. The 1.3 kHz frequency is just below one-half of the local electron cyclotron frequency at that time. Although broadband data are not available for the 0200-0300 UT period of Fig. 2 to assist in the identification, the emissions are most likely discrete emissions propagating in the whistler-mode. Although hiss is more likely to occur at that local time, the emission is not as constant in amplitude as typical hiss emissions.

Since the other cases show virtually no emissions prior to the plasma injection we conclude that the inner region of the plasma sheet is essentially quiescent. The frequency range up to 10 kHz includes both whistler-mode emissions and electrostatic cyclotron emissions in pass bands between electron cyclotron frequency harmonics. Neither are generally observed within this inner region of the plasma sheet prior to a substorm.

Signals above and below the electron cyclotron frequency start abruptly at the time of each plasma injection. In the data from the narrowband channels, the signature for each case is essentially the same. At the time the injected plasma encounters the satellite there is an abrupt increase in wave intensity in all channels from 400 Hz to 10 kHz. In most cases the waves at 10 kHz are weak.

The wave modes for each of the four cases can be identified using the broadband VLF spectrograms shown in Fig. 7. The identification uses the electron cyclotron frequency to distinguish whistler-mode waves below f_c^- from

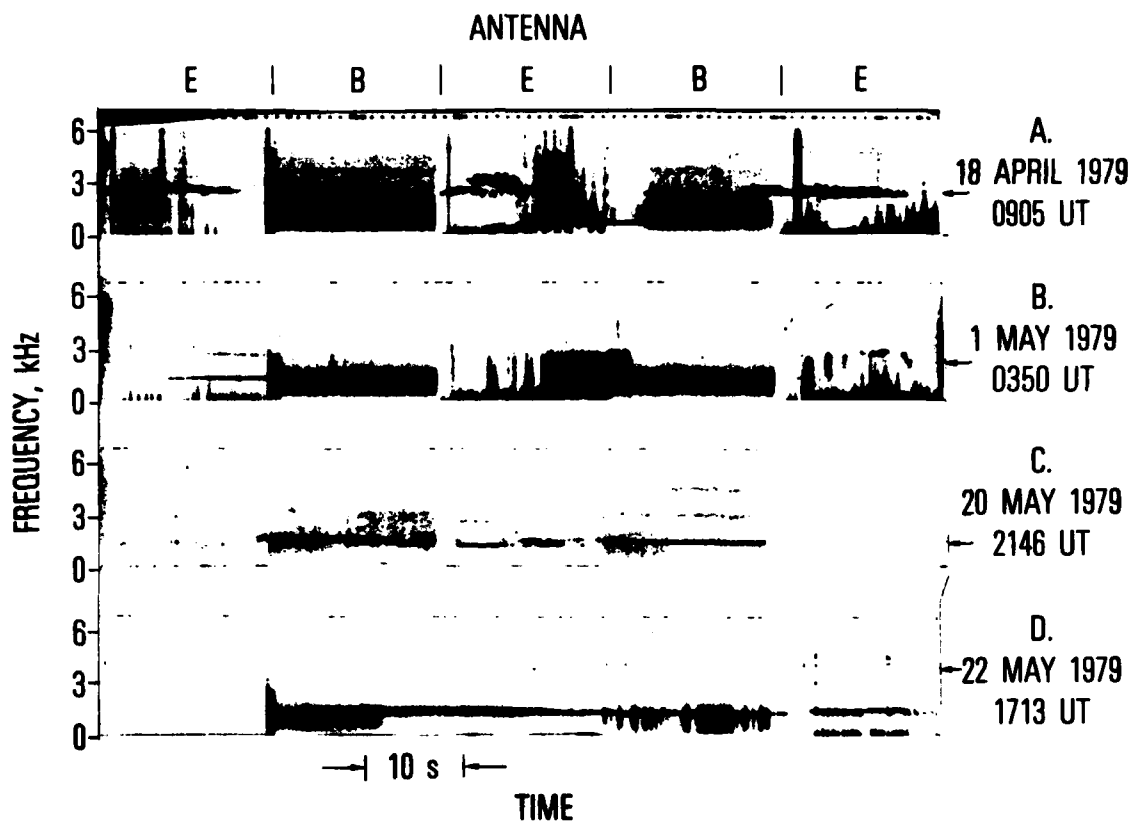


Fig. 7. Gray scale spectrograms of the VLF wave spectrum during the plasma injections described in this paper. An increase in darkness corresponds to an increase in wave intensity. Each 16 s the antenna switches between the electric antenna (E) and the magnetic antenna (B). Cross-talk exterior to the VLF wave instrument causes intense electrostatic emissions to appear in the data from the magnetic antenna. The electron cyclotron frequency is indicated by an arrow on the right side of each spectrogram. The values for the four cases are (a) 2380 Hz, (b) 2100 Hz, (c) 1764 Hz, and (d) 3836 Hz.

electrostatic emissions above f_c^- . The identification is based on a comparison of these spectrograms with over 1000 hours of others from the SCATHA satellite. Three types of signals appear on these spectrograms. The vertical lines in the electric antenna data in cases A and B are pulses due to electrical discharges. Surface materials on the vehicle were being charged to different potentials by the injected energetic electrons (P. Mizera, private communication, 1982). Electrical discharges between different surfaces produced the pulses in the VLF data. In cases A, B and C narrowband emissions appear just above f_c^- . These emissions are electrostatic electron cyclotron waves. Harmonics of the fundamental emission frequency can be seen in the spectrograms for cases A and C. In case D the upper frequency of the receiver passband (4 kHz at that time) was near the electron cyclotron frequency. The electrostatic cyclotron emissions would then be above the passband of the broadband receiver. The narrowband data, which shows weak emissions in the 10-kHz channel, indicates that the electrostatic cyclotron waves were present. Thus these waves occurred during each plasma injection.

Strong whistler-mode emissions below the electron cyclotron frequency appear in the broadband data in cases A, B and D. The whistler-mode waves bear little resemblance to discrete emissions such as chorus or incoherent emissions such as hiss. Chorus emissions are detected several hours after the substorm injections (Isenberg et al., 1982). On April 18 (Fig. 1) chorus occurs at 1.3 kHz from 1700 to 2200 UT (5.6 to 9.8 hr Local Time). On May 1 (Fig. 2), stronger chorus emissions are detected at 1.3 and 2.3 kHz from 1900 to 2100 UT (11.3 to 14.1 hr Local Time). On May 20 and 22 the substorms occurred at the end of the day and chorus was detected during the local morning hours on the following day. The low-frequency, narrowband signals near the baseband in case B are due to the electrical discharges. In case C the low-frequency signals cannot be identified. In that case the broadband data terminated shortly after the plasma injection. Up to the time the case C data terminated neither discharges nor whistler-mode emissions were detected. An instrument monitoring surface potentials measured differential potentials up to 1 kV between a Kapton sample and the space vehicle frame.

This potential is usually sufficient to produce the low-intensity discharges detected by the VLF receiver.

In summary then there were essentially no emissions present within the plasma sheet prior to a plasma injection. Following the injection there were in all cases electrostatic electron cyclotron waves. In three of the four cases there were narrowband structured whistler-mode emissions. In two cases there were also electrical discharges detected by the VLF receiver.

III. ELECTRON DISTRIBUTION FUNCTIONS

The electron distribution functions, $f(v)$, for sample time periods during each of the four cases are shown in Figures 8-11. For each case four distribution functions are shown as contours of constant phase space density in velocity space. The first, (a), shows the distribution function as the satellite enters the inner edge of the plasma sheet. The second, (b), was 15 to 60 minutes later after the satellite had penetrated a significant distance into the plasma sheet. The third, (c), shows the distribution function just prior to the plasma injection. The fourth, (d), distribution function in each set was obtained shortly after the injection and represents an equilibrium state for the plasma after the injection. Rapid variations in the direction of the magnetic field during the injection usually make it impractical to obtain the full one-minute of data required to obtain a complete quasistatic distribution function. Note that in nearly all cases the plasma analyzer's field of view did not include the magnetic field line direction. The gaps in the $f(v)$ contours near the v_{\parallel} axis in Figs. 8-11 indicate the closest approach of the field-of-view axis to the field line direction.

The electron distribution function, prior to entry into the plasma sheet, is a nearly isotropic soft (cold) spectrum. As the satellite penetrates into the plasma sheet the low energy electron ($E_e > 80$ eV) fluxes gradually increase. This low energy population is also soft but intense (ref. Figs. 8a-11a) as evidenced by the high density of iso- $f(v)$ contours near $v \leq 2 \times 10^4$ km/sec. This is also borne out by the sample energy spectra for cases A and B in Fig. 12a (upper and lower panels, respectively). At this point, the electron spectra are anisotropic with $J_{\perp} > J_{\parallel}$ at all energies. As the satellite penetrates further into the plasma sheet the spectrum, Fig. 12b (upper and lower) hardens and the intensity increases. This is especially apparent for particle pitch angles near 90° . In velocity space the dense central $f(v)$ contours spread out toward higher velocities (Ref. Figs. 8b-11b). At intermediate energies J_{\perp} continues to increase over J_{\parallel} .

18 APRIL 1979

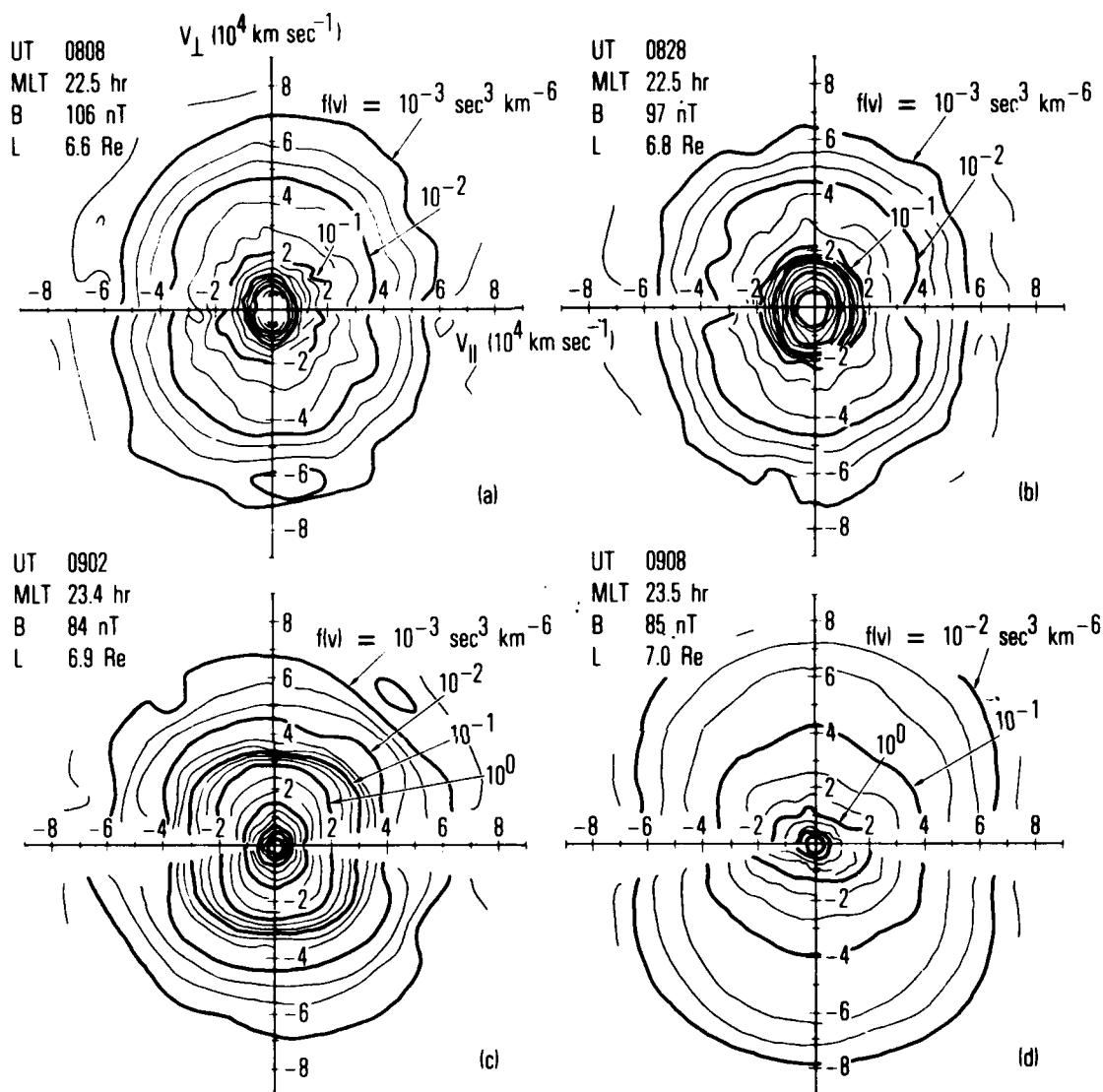


Fig. 8. Iso-distribution function, $f(v)$, contours in velocity space taken on April 18, 1979, (a) as the satellite enters the plasma sheet, (b) at an intermediate position in the plasma sheet, (c) just prior to the plasma injection, and (d) just after the injection. Every decade in $f(v)$ is indicated as a bold line. These plots each represent ~ 1 minute of data.

1 MAY 1979

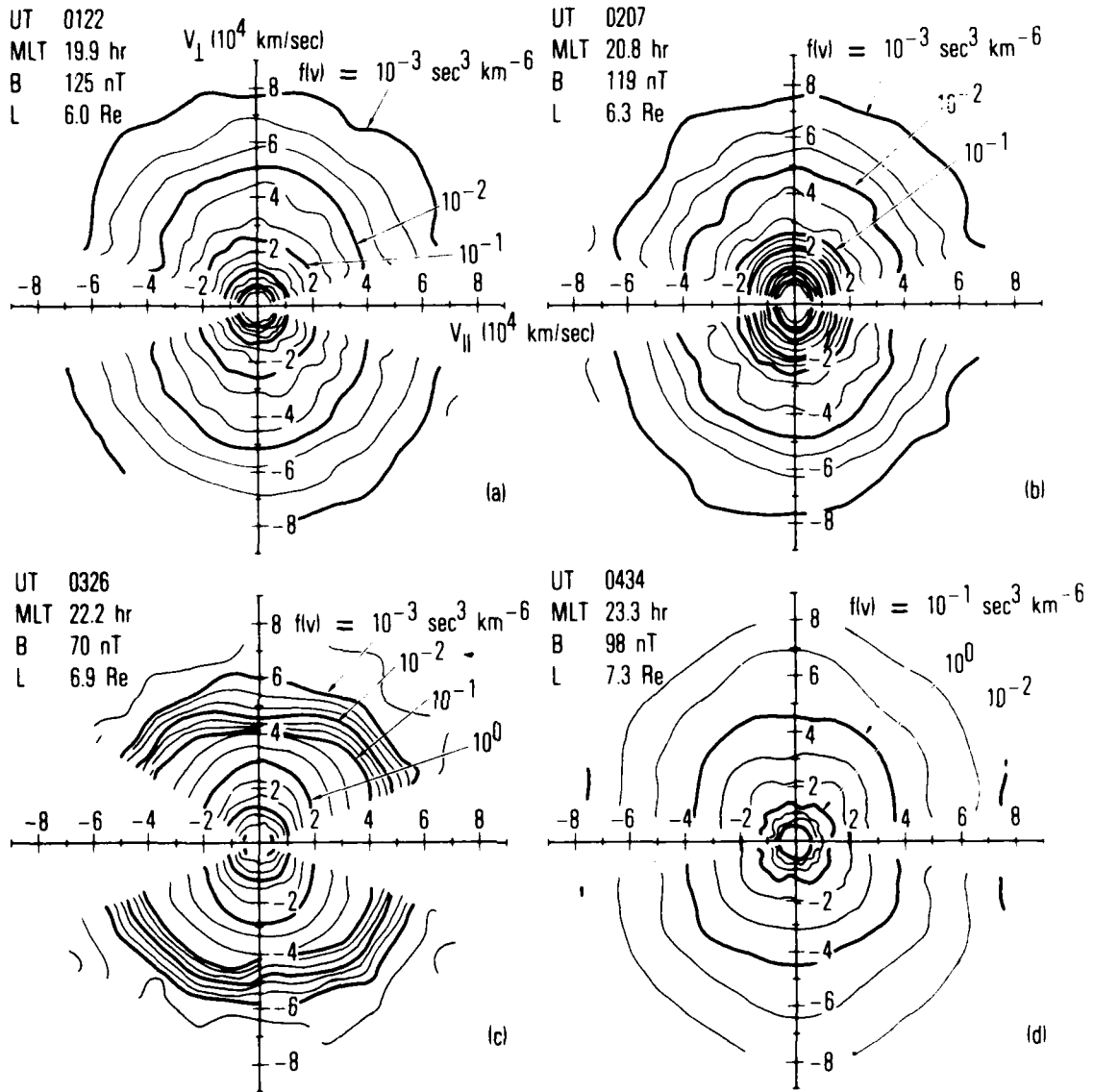
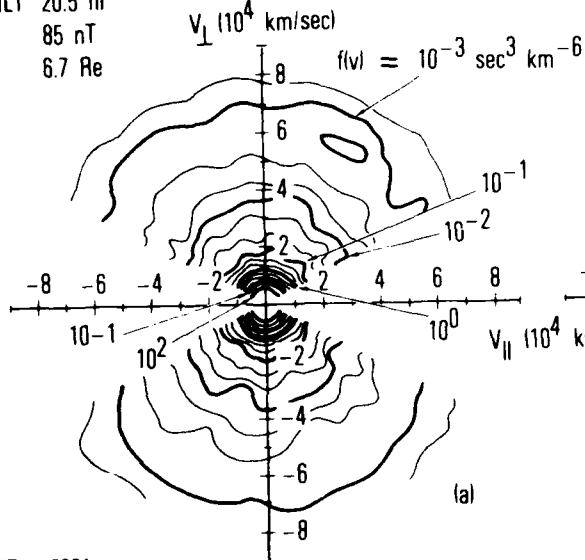


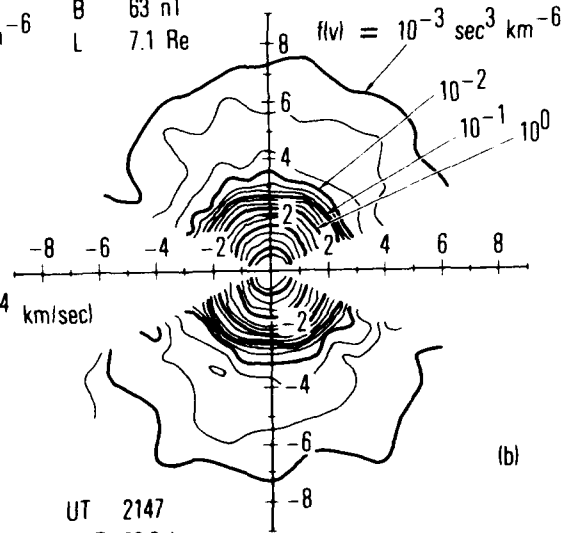
Fig. 9. Same as Fig. 9 for May 1, 1979.

20 MAY 1979

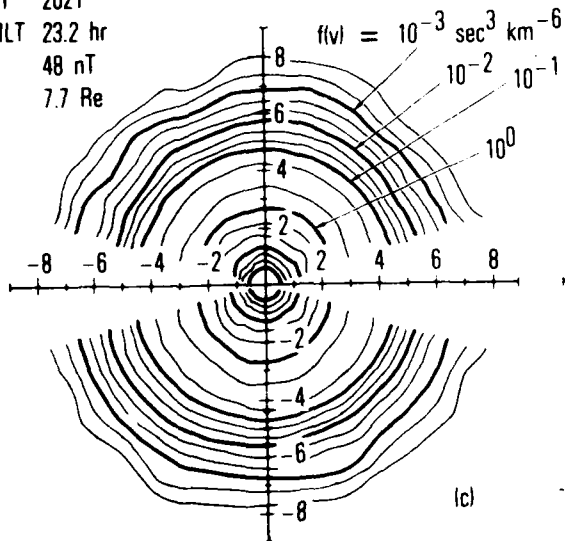
UT 1904
MLT 20.5 hr
B 85 nT
L 6.7 Re



UT 2001
MLT 21.6 hr
B 63 nT
L 7.1 Re



UT 2021
MLT 23.2 hr
B 48 nT
L 7.7 Re



UT 2147
MLT 23.2 hr
B 63 nT
L 7.7 Re

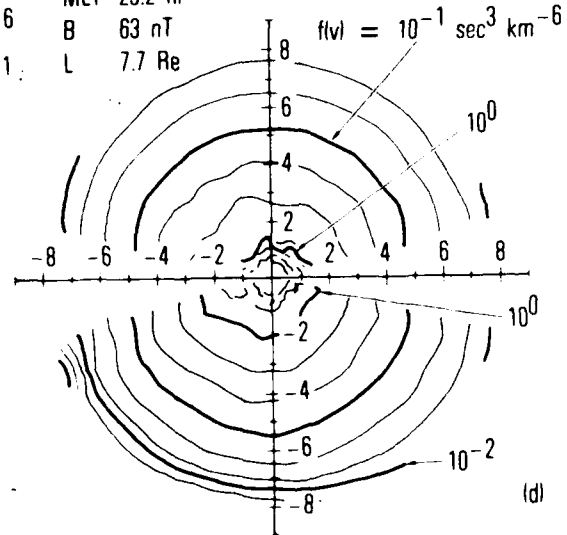


Fig. 10. Same as Fig. 9 for May 20, 1979.

22 MAY 1979

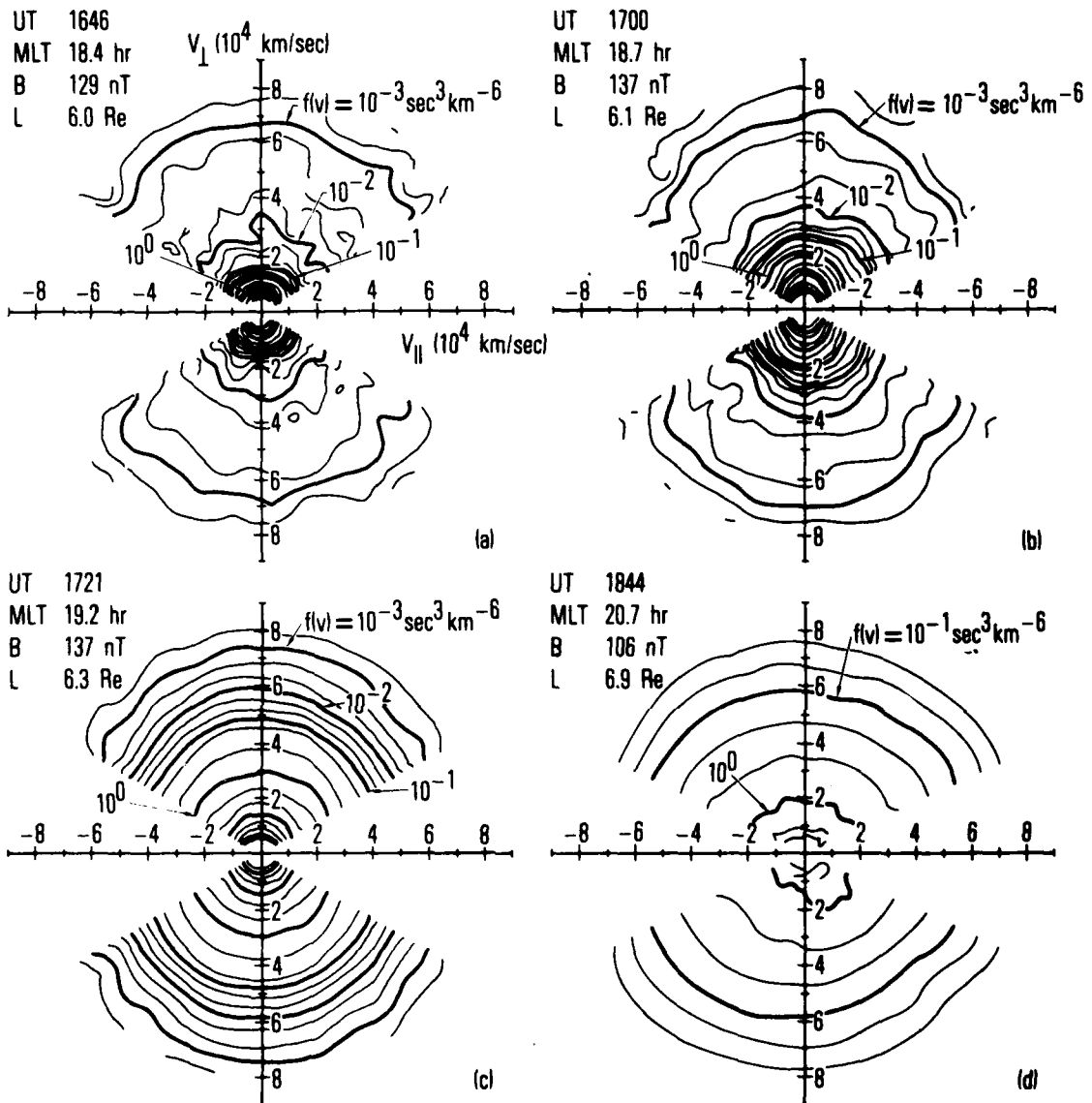


Fig. 11. Same as Fig. 9 for May 22, 1979.

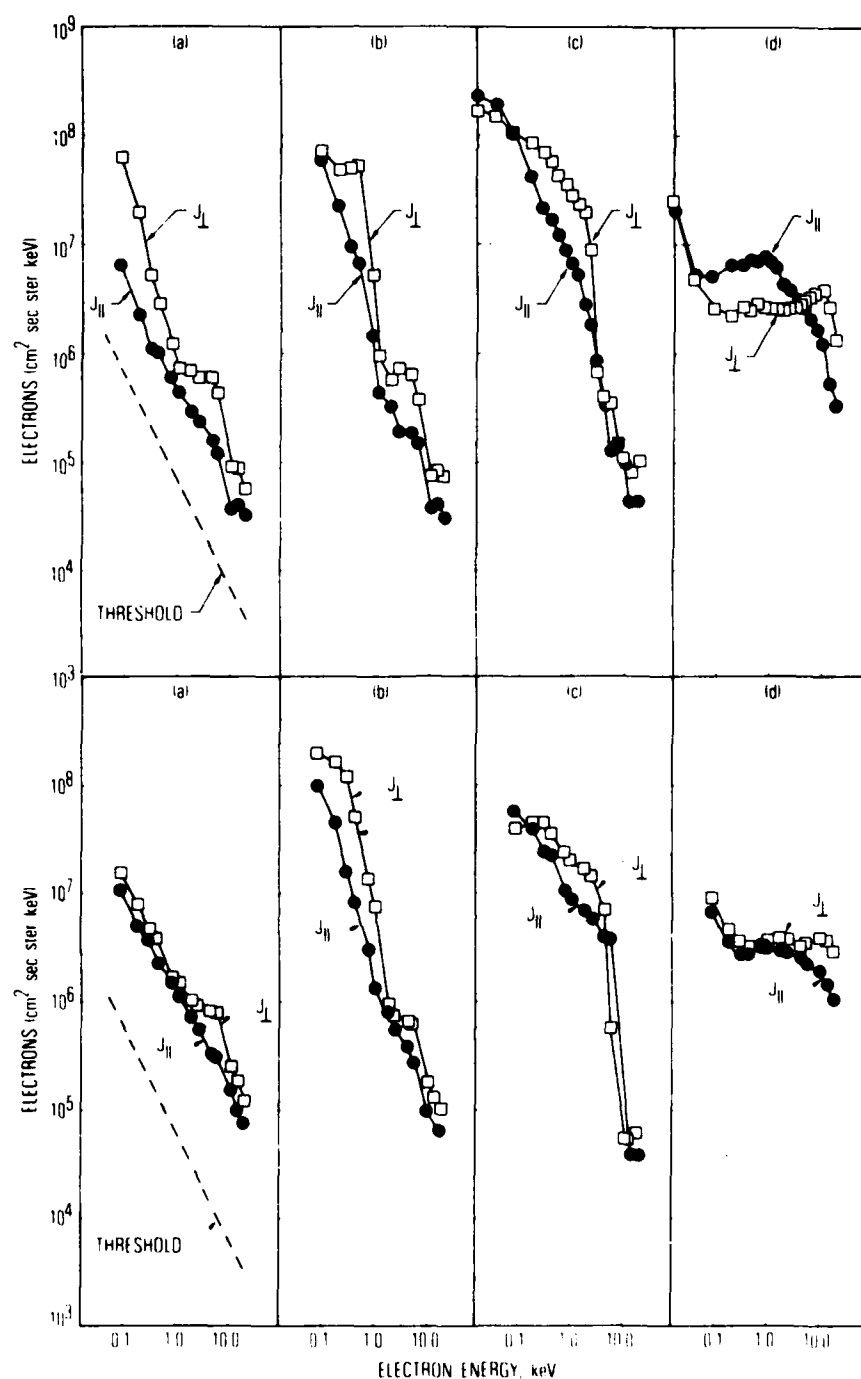


Fig. 12. Electron energy spectra. Top - April 18, 1979. The panels (a) through (d) correspond to data taken at the same times as those in Figs. 9a through 9d. The square points correspond to data taken near 90° pitch angle, and the solid dots correspond to data taken closest to the magnetic field direction. The instrument threshold is shown in (a) for reference. Bottom - May 1, 1979. Note that $J_{\parallel} > J_{\perp}$ near 6-8 keV in panel (c).

Prior to the injection, in a limited energy range associated with a steep negative gradient in $f(v)$, a pronounced minimum is often observed in the distribution function near $\alpha_0 = 90^\circ$. This feature is evident in Figs. 8 and 9 near $v_\perp \sim 3 \times 10^4$ km/sec and $\sim 4 \times 10^4$ km/sec respectively. It is also shown in Fig. 12c (upper and lower) by the fact that $J_\parallel > J_\perp$ over a narrow range of energies near 6-10 keV.

Figure 13 shows the individual angular distributions taken on 1 May 1979 near 0325 UT. These data are comparable to those of Fig. 9c and Fig. 12c (lower panel). The deep minima in the distributions near $\alpha \sim 90^\circ$ for electrons of 4.5 to 10.9 keV energy is obvious. The satellite is near 3.5 deg magnetic latitude (from model field discussed above). For 5.9 keV electrons the minimum at $\alpha \sim 90^\circ$ is $\sim 20\%$ of the peak value near $\alpha \sim 45^\circ$. This minimum would disappear for magnetic latitudes near 15 deg (based on a dipole magnetic field model) and would have an intensity $\sim 50\%$ of the equatorial value near a latitude 7.5 deg. Thus this "butterfly" distribution exists only near the magnetic equator. This feature is most likely caused by the normal convection process in the plasma sheet. Particles of a given energy with small pitch angles are expected to penetrate slightly closer to the earth than particles with pitch angles near 90° [Cowley and Ashour-Abdalla, 1975, 1976; Ejiri, 1978]. The corresponding energy spectra in Fig. 12c (lower panel) show a crossover of J_\perp and J_\parallel along the steep gradient in J with energy, representing the high-energy boundary of the plasma sheet.

This "butterfly" or "anti-loss-cone," as it is also called (Kennel and Ashour-Abdalla, 1982), angular distribution feature is a relatively common one in the SCATHA plasma sheet data. Strong electrostatic waves are often seen at the same time this feature is observed in the electron distribution. In these two cases very weak electrostatic electron cyclotron emissions were present prior to the injection. These waves are apparent in the broadband data but their amplitude is near the threshold of the narrowband receiver.

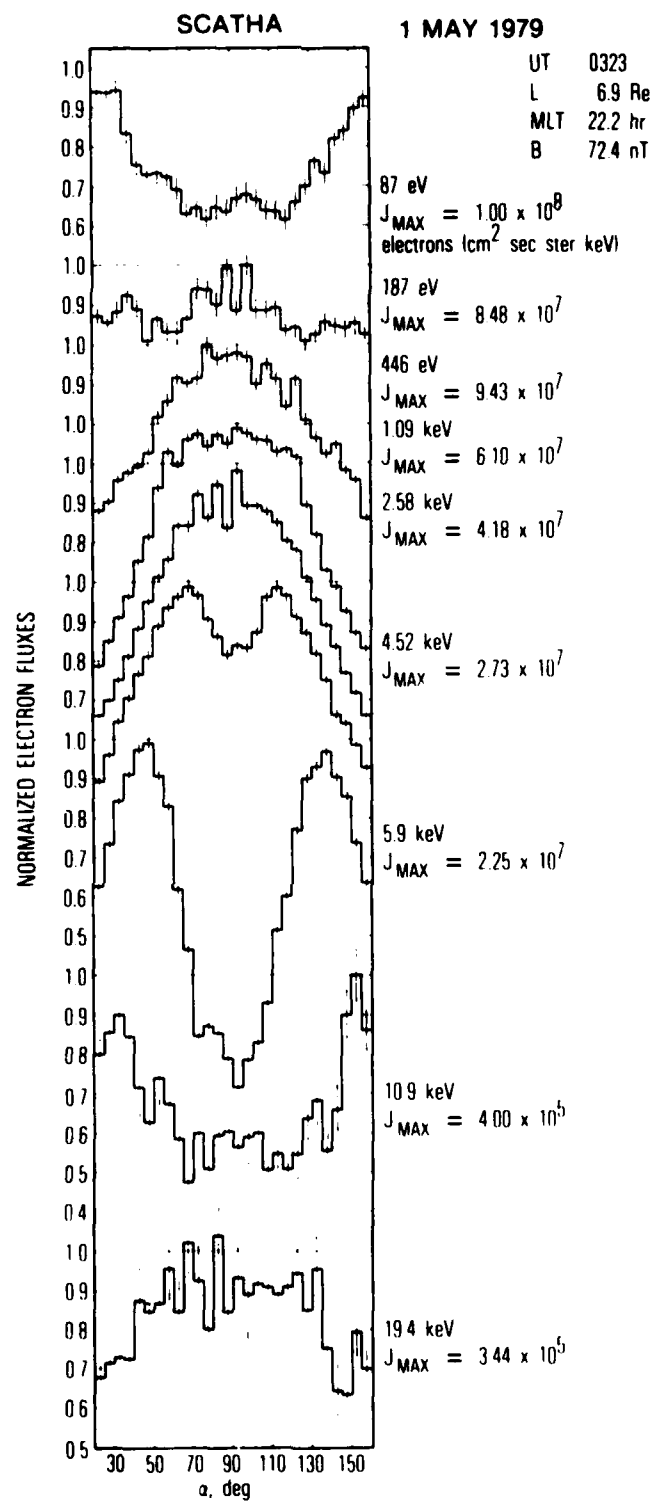


Fig. 13. Electron pitch-angle distributions taken near 0325 UT on May 1, 1979. Note the deep anti-loss-cone in the 4.5 to 10.9 keV distributions.

IV. SUMMARY

The present set of observations can be summarized as follows.

- 1) Before a substorm, plasma sheet electron distributions are usually stable with little evidence of electrostatic electron cyclotron harmonic emissions ($n + 1/2$ type waves) f_c^- .
- 2) Strong ($n + 1/2$) f_c^- type waves are observed at the substorm injection time and for a period following injection.
- 3) When preinjection ($n + 1/2$) f_c^- waves are observed they are often accompanied by "butterfly" or "anti-loss-cone" distributions in the keV energy electrons at the steep gradient in $f(v)$. The gradient is probably convection related.
- 4) Other types of wave noise such as whistler-mode waves and pulses due to discharges on the vehicle are also observed in conjunction with the plasma injection.

The particle distribution functions observed during these injections do not have the sources of free energy found by Kurth [1980] and Rönmark [1978], nor are they similar to the distribution functions which have been used for theoretical studies [Kennel and Ashour-Abdalla, 1982].

The source of free energy may be the anti-loss-cone feature which results from the pitch-angle dependent convection in the plasma sheet. The stability of an anti-loss-cone distribution function has been examined by Nambu and Watanabe [1975]. They did obtain instability slightly above the electron cyclotron frequency, however they assumed a temperature anisotropy of 10 which is not representative of the plasma sheet particle distributions measured by instrument aboard the SCATHA satellite. It is beyond the scope of this paper to analyze the measured particle distribution functions for instability to electron cyclotron harmonic waves.

REFERENCES

- Akasofu, S. -I. and J. R. Kan, Dayside and Nightside Auroral Arc Systems, Geophys. Res. Lett., 7, 753, 1980.
- Cowley, S. W. H. and M. Ashour-Abdalla, Adiabatic Plasma Convection in a Dipole Field: Variation of Plasma Bulk Parameters with L, Planet. Space Sci., 23, 1527, 1975.
- Cowley, S. W. H. and M. Ashour-Abdalla, Adiabatic Plasma Convection in a Dipole Field: Electron Forbidden-zone Effects for a Simple Electric Field Model, Planet. Space Sci., 24, 805, 1976.
- Barrachlough, D. R., J. M. Hardwood, B. R. Leaton and S. R. C. Malin, A Model of the Geomagnetic Field at Epoch 1975, Geophys. J. R. Astr. Soc. 43, 645, 1975.
- Ejiri, M., Trajectory Traces of Charged Particles in the Magnetosphere, J. Geophys. Res., 85, 4798, 1978.
- Fennell, J. F., Description of P78-2 (SCATHA) Satellite and Experiments, in The IMS Source Book, edited by Russell and Southwood, Am. Geophysical Union, Wash. D.C., 1982.
- Isenberg, P. A., H. C. Koons and J. F. Fennell, Simultaneous Observations of Energetic Electrons and Dawnside Chorus in Geosynchronous Orbit, J. Geophys. Res., 87, 1495, 1982.
- Kennel, C. F., F. L. Scarf, R. W. Fredricks, J. H. McGehee and F. V. Coroniti, VLF Electric Field Observations in the Magnetosphere, J. Geophys. Res., 75, 6136, 1970.
- Kennel, C. F. and M. Ashour-Abdalla, Electrostatic Waves and the Strong Diffusion of Magnetospheric Electrons, in Magnetospheric Plasma Physics, edited by A. Nishida, D. Reidel Publishing Co., Boston, MA, 1982, p. 245.
- Kivelson, M. G., S. M. Kaye and D. J. Southwood, The Physics of Plasma Injection Events, in Dynamics of the Magnetosphere, ed. S. I. Akasofu, D. Reidel Pub. Co., Boston, MA. p. 385, 1980.
- Koons, H. C., Role of Hiss in Magnetospheric Chorus Emissions, J. Geophysics Res., 86, 6745, 1981.
- Kurth, W. S., J. D. Craven, L. A. Frank and D. A. Gurnett, Intense Electrostatic Waves Near the Upper Hybrid Resonance Frequency, J. Geophys. Res., 84, 4145, 1979.

- Kurth, W. S., L. A. Frank, M. Ashour-Abdalla, D. A. Gurnett and B. G. Burek, Observations of a Free-energy Source for Intense Electrostatic Waves, Geophys. Res. Lett., 7, 293, 1980.
- Lyons, L. R., Electron Diffusion Driven by Magnetospheric Electrostatic Waves, J. Geophys. Res., 79, 575, 1974.
- Mauk, B. and C. E. McIlwain ATS-6 UCSD auroral particles experiments, IEEE Transactions on Aerospace and Electronic Systems, AES-11, 1125, 1975.
- Nambu, M. and T. Watanabe, Electrostatic Electron-cyclotron Waves With an Anti-loss-cone Distribution Function, Geophys. Res. Lett., 2, 176, 1975.
- Olsen, R. C., Equatorially Trapped Plasma Populations, J. Geophys. Res., 86, 11235, 1981.
- Olson, W. P., and K. A. Pfizter, A Quantitative Model of the Magnetospheric Magnetic Field, J. Geophys. Res., 79, 3739, 1974.
- Rönmark, K., H. Borg, P. J. Christensen, M. P. Gough and D. Jones, Banded Electron Cyclotron Harmonic Instability - A First Comparison of Theory and Experiment, Space Sci. Rev., 22, 401, 1978.
- World Data Center C2 for Geomagnetism, Data Book #5, Kyoto Univ., Japan, 1982.

LABORATORY OPERATIONS

The Laboratory Operations of The Aerospace Corporation is conducting experimental and theoretical investigations necessary for the evaluation and application of scientific advances to new military space systems. Versatility and flexibility have been developed to a high degree by the laboratory personnel in dealing with the many problems encountered in the nation's rapidly developing space systems. Expertise in the latest scientific developments is vital to the accomplishment of tasks related to these problems. The laboratories that contribute to this research are:

Aerophysics Laboratory: Launch vehicle and reentry fluid mechanics, heat transfer and flight dynamics; chemical and electric propulsion, propellant chemistry, environmental hazards, trace detection; spacecraft structural mechanics, contamination, thermal and structural control; high temperature thermomechanics, gas kinetics and radiation; cw and pulsed laser development including chemical kinetics, spectroscopy, optical resonators, beam control, atmospheric propagation, laser effects and countermeasures.

Chemistry and Physics Laboratory: Atmospheric chemical reactions, atmospheric optics, light scattering, state-specific chemical reactions and radiation transport in rocket plumes, applied laser spectroscopy, laser chemistry, laser optoelectronics, solar cell physics, battery electrochemistry, space vacuum and radiation effects on materials, lubrication and surface phenomena, thermionic emission, photosensitive materials and detectors, atomic frequency standards, and environmental chemistry.

Computer Science Laboratory: Program verification, program translation, performance-sensitive system design, distributed architectures for spaceborne computers, fault-tolerant computer systems, artificial intelligence and microelectronics applications.

Electronics Research Laboratory: Microelectronics, GaAs low noise and power devices, semiconductor lasers, electromagnetic and optical propagation phenomena, quantum electronics, laser communications, lidar, and electro-optics; communication sciences, applied electronics, semiconductor crystal and device physics, radiometric imaging; millimeter wave, microwave technology, and RF systems research.

Materials Sciences Laboratory: Development of new materials: metal matrix composites, polymers, and new forms of carbon; nondestructive evaluation, component failure analysis and reliability; fracture mechanics and stress corrosion; analysis and evaluation of materials at cryogenic and elevated temperatures as well as in space and enemy-induced environments.

Space Sciences Laboratory: Magnetospheric, auroral and cosmic ray physics, wave-particle interactions, magnetospheric plasma waves; atmospheric and ionospheric physics, density and composition of the upper atmosphere, remote sensing using atmospheric radiation; solar physics, infrared astronomy, infrared signature analysis; effects of solar activity, magnetic storms and nuclear explosions on the earth's atmosphere, ionosphere and magnetosphere; effects of electromagnetic and particulate radiations on space systems; space instrumentation.

END

FILMED

2-86

DTIC